Orographic Influences on the Distribution and Generation of Atmospheric Variability in a GCM

JIN-YI YU* AND DENNIS L. HARTMANN

Department of Atmospheric Sciences, University of Washington, Seattle, Washington

(Manuscript received 24 February 1994, in final form 24 January 1995)

ABSTRACT

The effect of large-scale mountains on atmospheric variability is studied in a series of GCM experiments in which a single mountain is varied in height from 0 to 4 km. High-frequency ($\tau < 7$ days) and low-frequency ($\tau > 30$ days) variability are largest in the jet exit region, while the intermediate-frequency ($7 < \tau < 30$ days) variability has its maximum upstream of the mountain where it exhibits enhanced equatorward propagation. High and intermediate frequencies change from zonal wave trains to localized wave packets as orographic forcing is increased, but they retain their characteristic scale and frequency. The dominant pattern of low-frequency variability changes from a zonally symmetric oscillation, for which transient eddy-zonal flow interaction is the dominant mechanism, to a more localized oscillation of the jet downstream of the mountain. The transient eddy forcing still plays a significant role in maintaining the variations of this more localized jet, however.

The total amount of wave energy remains almost constant as the mountain height is increased, but the distribution of wave energy shifts from transient to stationary and from high frequencies to low frequencies. Low-frequency variability shows a step function response to orographic forcing in that it shows no response to a 1-km mountain, increases substantially in response to a 2-km mountain, and then shows little further increase as the mountain is raised to 3 and 4 km. This behavior suggests that the mechanism that generates the additional low-frequency variability in the mountain-forced experiments becomes effective after the zonal asymmetry reaches a critical value and then does not respond much to further increases in asymmetry.

1. Introduction

The appearance of strong zonally asymmetric components is a major difference of the Northern Hemisphere circulation from that of the Southern Hemisphere. The maintenance of these stationary waves has been attributed to thermal forcing, orographic forcing, and transient eddy forcing. Among them orographic forcing from the Himalaya and Rocky Mountain ranges is considered the dominant contributor, especially for the wintertime circulation (Wallace 1983). The importance of orographic forcing in the time-mean circulation is well known, but it is less clear what role orography plays in the temporal variation of atmospheric circulation. It is reasonable to suppose that continuous forcing from underlying large-scale mountains has a significant influence on the variation of atmospheric circulation. This study is aimed at a better understanding of how the distribution and generation of atmospheric variability is affected by the inclusion of an idealized large-scale mountain.

Orography can influence the generation or propagation of atmospheric variability directly through interaction between mountains and transient eddies or indirectly through the orographically forced stationary waves. One example of direct influence of mountains on eddy propagation is the study of Hsu and Wallace (1985). They analyzed the vertical structures of low-frequency variability in the vicinity of the Himalayas and the Rockies and noticed that the propagation of these transient eddies is affected by the large-scale mountains. Similar steering of high-frequency transients by orography was also observed by Hsu (1987). The formation of orographically forced stationary waves has even wider influences on the transient activity. The atmospheric instabilities in a zonally asymmetric basic state are different from those in a zonally symmetric state, and certain locations are more favorable for the growth of eddies with particular timescales. The linkage between the baroclinic instability of the zonally asymmetric mean flows and the localization of storm tracks has been one area of extensive studies (e.g., Frederiksen 1983; Pierrehumbert 1984). The barotropic instability of a zonally varying basic state is also very different from that of a zonally symmetric one. Simmons et al. (1983) showed that the unstable barotropic normal modes associated with the zonally

* Current affiliation: Department of Atmospheric Sciences, University of California, Los Angeles, Los Angeles, California.

Corresponding author address: Dr. Jin-Yi Yu, Department of Atmospheric Sciences, University of California, Los Angeles, 405 Hilgard Avenue, Los Angeles, CA 90024-1565.

asymmetric time-mean flow resemble some observed low-frequency patterns. The zonal gradient of the time-mean flow is as important as the meridional gradient in providing energy to the growth of the unstable barotropic modes. Besides their influences on wave generation, stationary waves also affect the propagation of transient eddies. Waveguides are formed in different locations for different scales of eddies (Branstator 1983; Hoskins and Ambrizzi 1993), and convergence of wave activity can influence the distribution of variability. So from the points of view of instability and wave propagation, large-scale mountains can affect both the generation and distribution of atmospheric variability indirectly through the forced stationary waves. Since various timescales of transients may be generated through different mechanisms and have different propagation characteristics, the effect of orography on variability will depend on the timescale.

The investigation of orographic influence on atmospheric variability is further complicated by the interference between orographic forcing and the internal dynamical processes. Hendon and Hartmann (1985) have shown in a two-layer GCM that low-frequency variations can be generated through the internal dynamics of the atmosphere. Yu and Hartmann (1993; YH93 hereafter) also showed that in their GCM the latitudinal location and the strength of zonal mean jet stream experience low-frequency variations as a result of interaction between the zonal flow and baroclinic eddy life cycles. Since the presence of orographic forcing can affect the generation and distribution of baroclinic eddies, the generation of low-frequency variability through internal dynamical processes will surely be influenced by orography and the zonal asymmetries it generates. In addition, internally generated low-frequency variations of jet stream structure can also interact directly with mountains and cause variations in the orographic forcing. So whether or not the total amount of low-frequency variance will be increased or decreased by the inclusion of orographic forcing will depend on both the internal dynamics and the orographic forcing mechanisms.

Hendon (1986) used a two-layer GCM to study the variability in an atmosphere above an idealized mountain, and concluded that the overall level of globally integrated transient activity is not affected by the presence of midlatitude orography. It is the longitudinal distribution of variance in his study which is strongly affected by the time–mean asymmetry in the basic state. His two-layer model uses pressure coordinates, in which orographic forcing is represented by an approximate sink–source term in the prognostic equations for relative vorticity and divergence. The full effects of orography, such as the mountain form drag and the direct interaction between mountain and transients, cannot be included. In our study, a sigma coordinate GCM is utilized to better incorporate orographic effects into the model atmosphere. The role of orographic forcing on the distribution and generation of atmospheric variability is investigated by varying the height of an idealized mountain.

2. Model and simulations

The GCM used for this study is the same one described in Yu and Hartmann (1993). Detailed development of this sigma coordinate GCM is described in Yu (1993). This is a dry primitive equation model with parameterized frictional damping, diabatic heating, and horizontal diffusion. A T21 spectral-transform method is used for the horizontal representation, and a 7-level finite-element method is adopted to represent the vertical structure. A 1-h time step was used with the semi-implicit scheme of Robert et al. (1972). An idealized mountain of Gaussian shape is placed in the Northern Hemisphere of the model, but no topography is present in the southern model hemisphere. The Gaussian-shaped mountain is prescribed as

$$Z = Z_0 e^{-\{[(\lambda-\lambda_0)/\Delta\lambda]^2+[(\phi-\phi_0)/\Delta\phi]^2\}}. \quad (1)$$

Here Z_0 is the height of the mountain; $(\lambda_0, \phi_0) = (180°\text{E}, 40°\text{N})$ are the centered longitude and latitude of the mountain; and $(\Delta\lambda, \Delta\phi) = (30°, 15°)$ are the widths of the mountain in longitude and in latitude. Four simulations with a mountain height Z_0 of 1, 2, 3, or 4 km were conducted for this study. The height of the northern hemisphere mountain is the only difference between these four simulations. Both the mountain and the no-mountain hemispheres are thermally relaxed toward the same equilibrium temperature which has a $\cos(2 \times \text{latitude})$ profile. The equator to pole temperature differences are about 60 K at most vertical levels, but a reverse temperature gradient with a temperature difference of 30 K is used at the top level. The GCM is spun up from an isothermal and resting state for 300 days, and day 300 is then used as the initial condition for another 3070 days of integration for analyses. In this paper, the southern hemisphere of the 4-km simulation is referred to as the no-mountain simulation for the purpose of comparison with the four mountain hemispheres.

3. Geographical distribution of atmospheric variability

The zonal asymmetry in the time mean zonal wind field is a qualitative measurement of the strength of orographic forcing. Comparisons among time-mean flows in the four mountain simulations (not shown) indicate that with a higher mountain in the simulation, the jet is not only more localized in structure but also stronger in its maximum wind speed. The mean zonal wind from the 4-km mountain simulation is shown in Fig. 1 for the 200-mb level, which is the jet stream level in the model. A localized jet appears about 60° downstream from the center of the mountain. If we take the

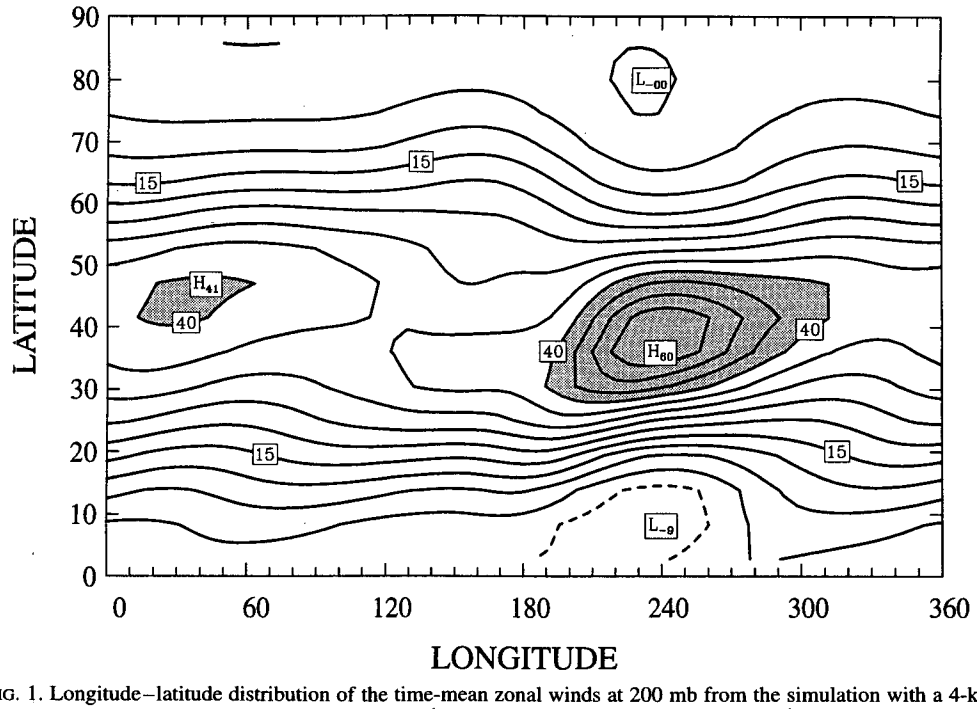

FIG. 1. Longitude–latitude distribution of the time-mean zonal winds at 200 mb from the simulation with a 4-km mountain. Contour intervals are 5 m s^{-1}, and wind speeds greater than 40 m s^{-1} are shaded.

4-km mountain to represent the Himalayas, then both the magnitude and the horizontal distribution of this upper-level wind are reasonable compared to the mean wintertime circulation in the Northern Hemisphere. So this GCM produces a reasonable time-mean response to orographic forcing.

Since Hendon (1986) showed that the zonal distribution of atmospheric variability is affected by the inclusion of orography, we first examined the orographic influences on the distribution of atmospheric variability. The power spectrum of 300-mb relative vorticity is calculated from the 3070 days of the 4-km mountain simulation. The power spectra are then smoothed by band-averaging over groups of 100 adjacent frequencies, over latitude from 20° to 70°N, and over two adjacent zonal grid points. The power spectrum, thus averaged, is shown in Fig. 2 as a function of longitude and frequency. Figure 2 shows strong zonal asymmetry in the variability distribution and indicates different orographic influences on different timescales of variability. To emphasize the zonal variations of variability for each timescale, "power ratios" are calculated from Fig. 2 and are shown in Fig. 3. The ratios are calculated by scaling the averaged powers at each frequency band in Fig. 2, with the zonal mean power in that frequency band. Variability at a particular frequency is more localized in the longitudes with higher power ratios and is suppressed in the regions of smaller ratio values. The variability with timescales shorter than 7 days is maximum in the jet exit region (340°). For variability with timescales longer than 30 days, the maximum power ratios tend to also be concentrated in the jet exit area. For timescales between 7 days and 30 days, the maximum variability is located at about 120°, which is the region just upstream of the mountain. The separation of different timescales of variability in Fig. 3 suggests that high- (periods less than 7 days), intermediate- (between 7 days and 30 days), and low-frequency (longer than 30 days) eddies are affected by large-scale mountains in different ways. But all temporal variability in midlatitudes is suppressed in the region of the jet core.

Figures 2 and 3 show that with the presence of a 4-km mountain, different timescales of variability are separated into various geographical locations. To find out how this zonal separation of variability is related to the strength of the orographic forcing, the zonal distributions of the high-, intermediate-, and low-frequency variabilities are compared among the four mountain simulations. Transient eddies are separated into the high-, intermediate-, and low-frequency components with 7-day and 30-day low-passed filters. Kinetic energy is calculated for each time scale, latitudinally averaged between 20° and 70°N, and mass-weighted from 1000 to 200 mb. The averaged transient kinetic energy from the no-mountain and the 1-, 2-, 3-, and 4-km mountain simulations are shown in Fig. 4. The suppression of transient kinetic energy in the jet entrance regions is obvious in the four mountain simulations, and the degree of suppression is increased with the height of the mountain. Transient energy in the mountain simulations is increased locally in the jet exit region for high- and low-frequency eddies and up-

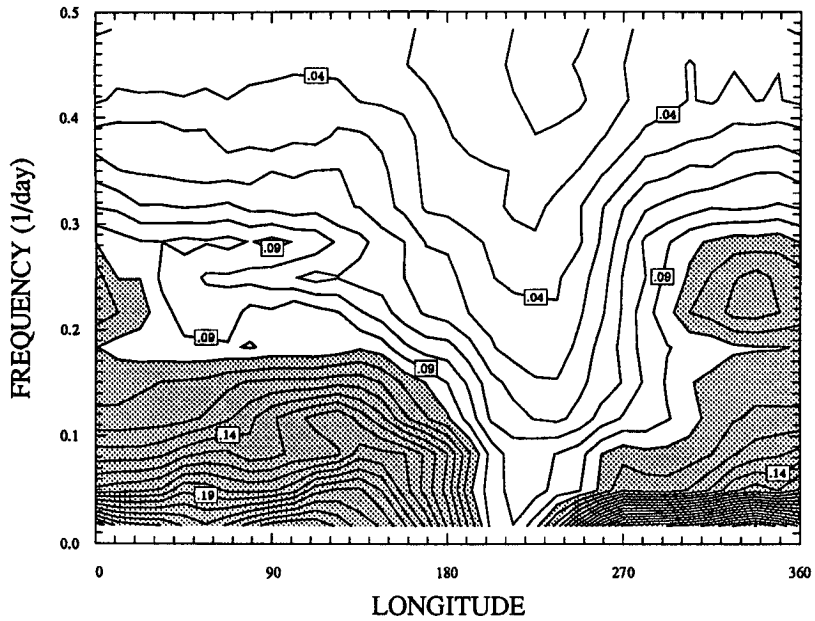

FIG. 2. Latitudinally averaged powers of the 300-mb relative vorticity from the 4-km mountain simulation, as a function of longitude and frequency. The powers are calculated from daily output and are averaged over 100 adjacent frequency bands. The powers are then averaged from 20° to 70°N and every two zonal grids. Contour interval is 1×10^{-14} s^{-2}, and contour labels are given in units of 10^{-12} s^{-2}. Powers larger than 10×10^{-14} s^{-2} are shaded.

stream of the mountain for the intermediate-frequency eddies. Figures 4a–c also suggest that the total amounts of transient kinetic energy vary with the mountain height. Orographic influences on the amount of variability will be discussed in section 5. The relation between the zonal asymmetry of the variability distribution and the strength of orographic forcing is better shown in Figs. 4d–f. In these three panels, the ratios of averaged transient kinetic energy with respect to their zonal mean values are shown. These panels

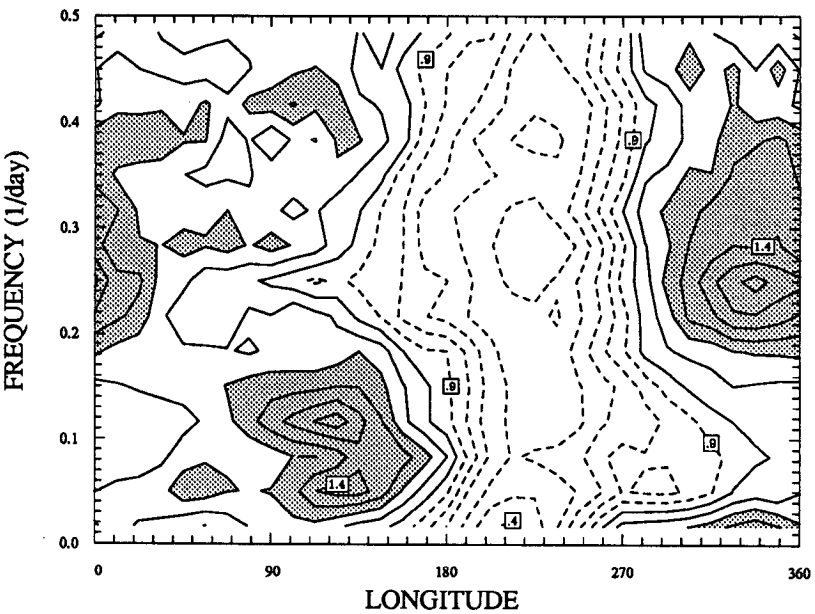

FIG. 3. Power ratios for the averaged power in Fig. 2. The calculation of power ratio is explained in the text. Contour interval is 0.1. Ratios larger than 1.2 are shaded, and ratios less than 1.0 are contoured by dash lines.

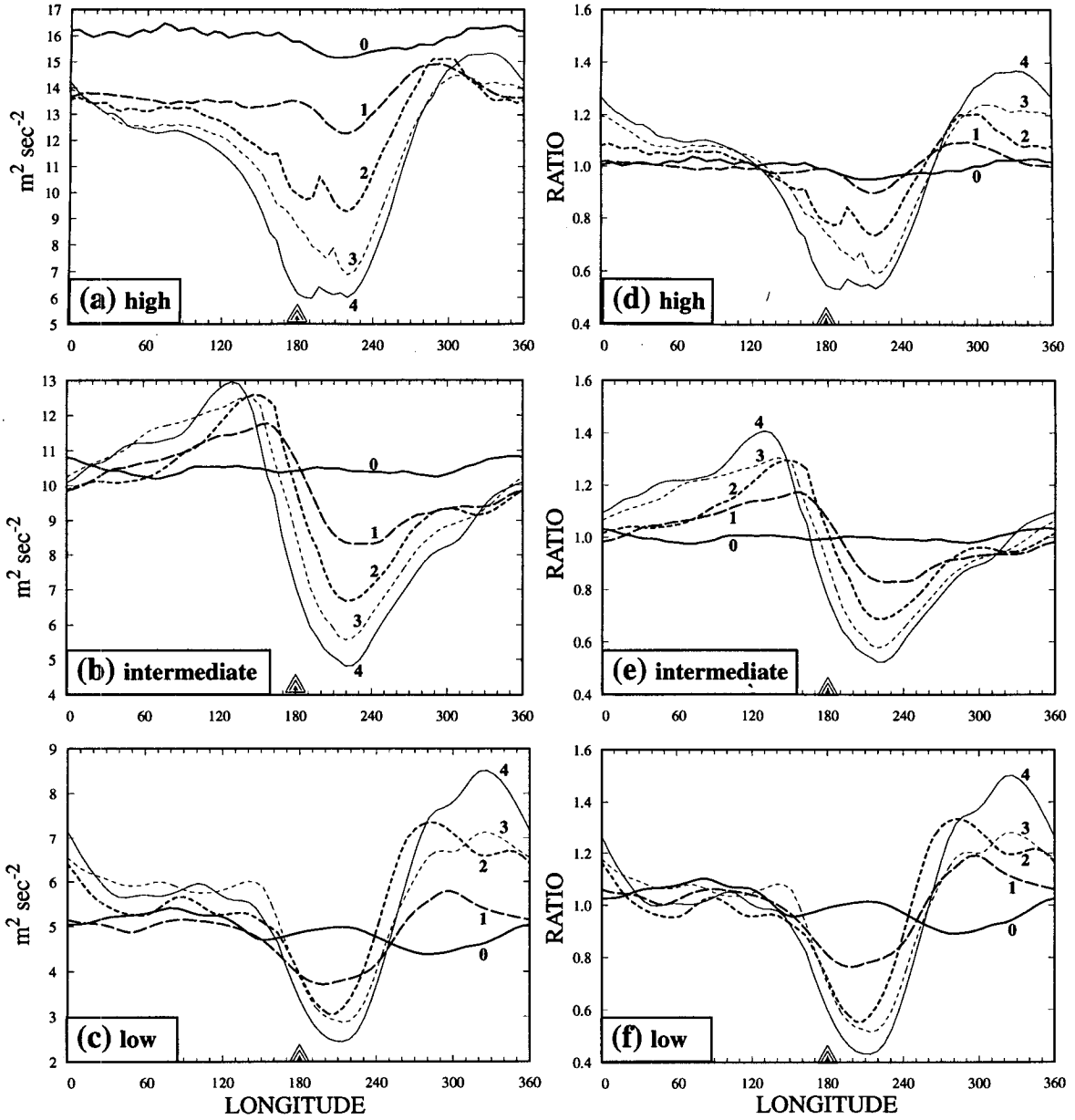

FIG. 4. Zonal distribution of the kinetic energy of high-, intermediate-, and low-frequency eddies from the mountain and the no-mountain simulations. (a), (b), (c) Eddy kinetic energy averaged between 20° and 70°N and mass-weighted from 1000 to 200 mb. (d), (e), (f) Ratios of these average kinetic energies to their zonal mean values. (a) and (d) For high-frequency transients; (b) and (e) for intermediate-frequency transients; and (c) and (f) for low-frequency transients. The number labeled near each curve indicates the height in kilometers of the mountain used in the simulation from which that curve is calculated.

clearly show that the degree of zonal asymmetry in variability distribution is positively correlated with the height of the mountain for all frequency bands. This relation indicates that it is indeed the orographic forcing and the zonal asymmetries it generates that separate variability of various timescales into different geographical regions.

The horizontal distributions of atmospheric variability for various timescales are shown in Fig. 5. In this figure, the transient eddy kinetic energy has been mass-weighted between 1000 and 200 mb. As seen in Fig. 4, the high- and intermediate-frequency variability are localized in the jet exit region and upstream of the mountain, respectively. The low-frequency variability exhibits a dumbbell-shaped maximum that straddles the jet exit. The geographical distributions of variability in this simple GCM are qualitatively similar to what has been observed in the atmosphere. Blackmon et al.

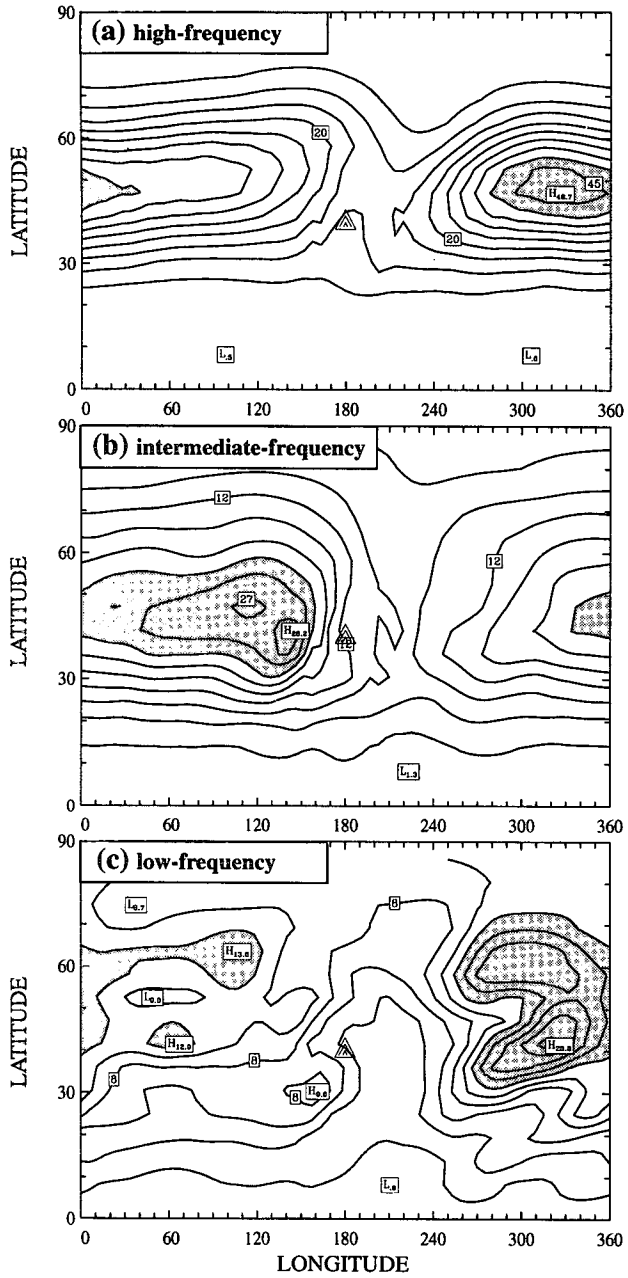

FIG. 5. Horizontal distributions of mass-weighted kinetic energy of (a) high-frequency, (b) intermediate-frequency, and (c) low-frequency transients from the 4-km mountain simulation. Contour intervals are 5 $m^2 s^{-2}$ in (a), 3 $m^2 s^{-2}$ in (b), and 2 $m^2 s^{-2}$ in (c). Shading is used to highlight local maxima.

(1983a,b) analyzed the 500-mb geopotential height fluctuations for the long, intermediate, and short timescales. Their results show that for the short timescale (2.5 ~ 6 days), the maximum variability is to the north of the jet stream. Most of the intermediate timescale fluctuations in the atmosphere appear in the entrance region of the jet stream and across the jet stream where they propagate equatorward. The entrance regions shown in Fig. 13 of Blackmon et al. (1983a) are actually located near and upstream of the Himalayas and the Rockies. Their studies also show that low-frequency variability is dominated by geographically fixed dipole patterns in the exit regions of two jets. The geographical distribution of variability in the 4-km mountain simulation is similar to the observed distribution of variability in the Northern Hemisphere.

4. Spatial patterns of transient eddies

a. High-frequency transients

To investigate the dominant patterns for high-frequency variability, EOF analysis was applied to the covariance matrix of high-frequency relative vorticity at 300 mb from the mountain simulations and the no-mountain simulation. It is noticed that the first few EOF modes appear in pairs. Each pair of EOF modes are 90° out of phase in space but closely correlated in a particular time lag. For example, the time-lag correlation coefficient (not shown) between the principal components of the first and the second EOF modes for the high-frequency 300-mb relative vorticity in the 4-km mountain simulation is almost one at one-day time lag. This pair of EOF modes actually represents a propagating pattern with a period of 4 days. The fraction of variance explained by this propagating pattern is the sum of the fractions of the two EOF modes, which is 20%.

The first pairs of propagating EOF modes from the no-mountain and the mountain simulations are compared in Fig. 6. In the no-mountain simulation, the dominant high-frequency eddy has a zonal wavenumber 6 pattern whose amplitude is almost independent of longitude. This is consistent with the results obtained by the time–space spectral analyses in YH93, which shows that the synoptic timescales in the no-mountain simulation are dominated by zonal wavenumber 6. The dominant patterns for high-frequency transients in the 1 or 2 km mountain simulations still have a zonal scale of zonal wavenumber 6, but it is evident that the amplitude of this pattern becomes less homogeneous in zonal direction, and the meridional tilts are changed in the region downstream of the mountain. In the case of the stronger orographic forcing represented by the 4-km mountain, the dominant pattern for high-frequency transients changes to a local wave packet with maximum amplitude within the storm track shown in Fig. 5a. The zonal and meridional scales of this local pattern are close to the patterns in the no-mountain simulation whose amplitudes are more zonally invariant. From the similarity of spatial structures shown in Fig. 6, we can argue that the main influence of orographic forcing on high-frequency transients is to modulate their amplitudes in the zonal direction. The amplitude modulation of the high-frequency eddies may be explainable in

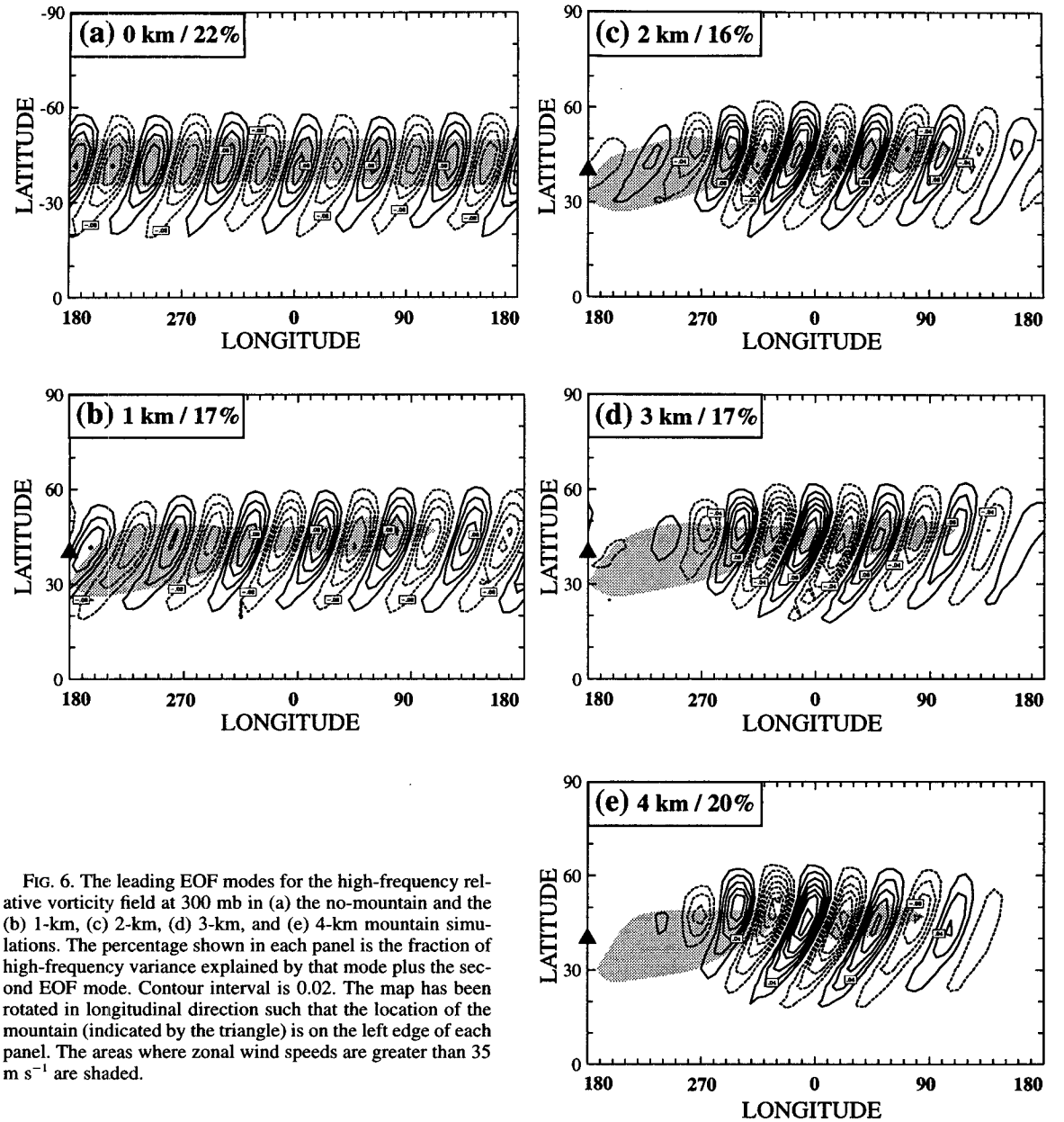

FIG. 6. The leading EOF modes for the high-frequency relative vorticity field at 300 mb in (a) the no-mountain and the (b) 1-km, (c) 2-km, (d) 3-km, and (e) 4-km mountain simulations. The percentage shown in each panel is the fraction of high-frequency variance explained by that mode plus the second EOF mode. Contour interval is 0.02. The map has been rotated in longitudinal direction such that the location of the mountain (indicated by the triangle) is on the left edge of each panel. The areas where zonal wind speeds are greater than 35 m s^{-1} are shaded.

terms of the baroclinic wave lifecycle. The stronger the stationary wave, the more localized the baroclinically unstable zone will be. Baroclinic waves grow in a limited region near the jet core, and they become fully developed and reach their maximum amplitudes in the jet exit region. In the jet exit region they become more barotropic and begin to decay as they propagate equatorward further downstream from the jet. The deformation suppression by the stationary wave, as suggested by Lee and Held (1993), may also enhance the amplitude modulation of high-frequency eddies when orographic forcing is increased.

b. Intermediate-frequency transient eddies

The first few EOF modes of the intermediate-frequency variability are also pairs of propagating waves. The leading EOF modes in each simulation are shown in Fig. 7. The leading mode in the no-mountain simulation (Fig. 7a) exhibits a global pattern with a zonal scale of wavenumber 5. This pair of propagating EOF modes explains 23% of the intermediate-frequency variability. The time-lag correlation between the principal component of the first and the second EOF modes (not shown) indicates that this eastward-propagating

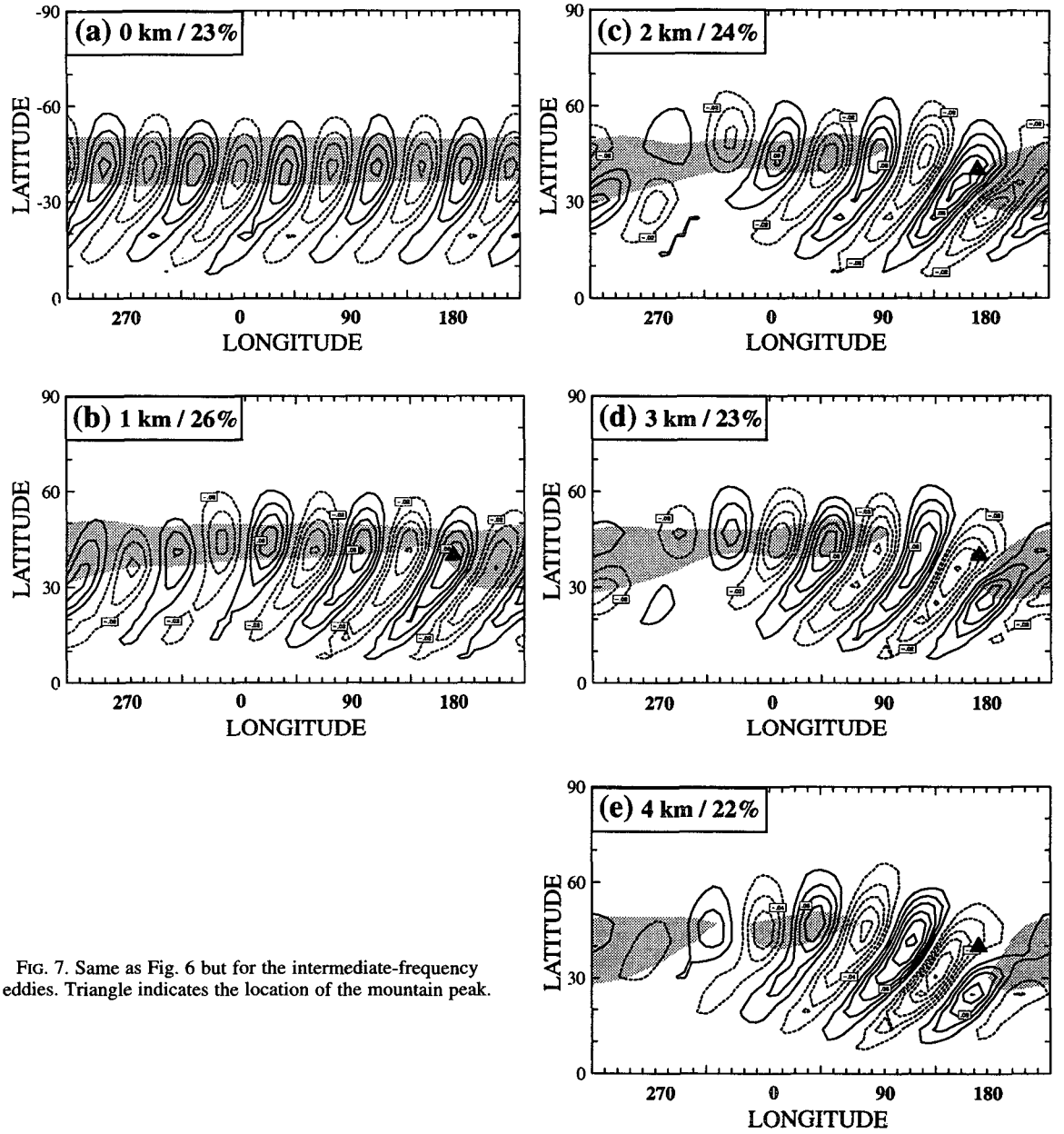

FIG. 7. Same as Fig. 6 but for the intermediate-frequency eddies. Triangle indicates the location of the mountain peak.

mode has a period of 10 days. These dominant time and space scales were seen in the time–space spectral analyses for the no-mountain hemisphere in YH93. With increasing orographic forcing of the model atmosphere, the amplitudes of the leading EOF modes become modulated in the zonal direction. The equatorward dispersion of these modes is also increased. A wave train pattern is seen in the 4-km mountain simulation as the dominant pattern for intermediate-frequency transients. The period of this wave train pattern is about 12 days (based on time-lag correlation analyses), which is a little longer than the period of the global pattern in the no-mountain case. But the zonal scale of this pattern is still close to zonal wavenumber 5. The wave train exhibits strong equatorward propagation near the upstream edge of the mountain and attains its maximum amplitude in the same area. It accounts for the maximum intermediate-frequency variability observed in Fig. 5b. This mode explains 22% of the intermediate-frequency variance, which is larger than the variance explained by the second pair of propagating EOF modes (14%). So a wave train pattern is the dominant structure of intermediate-frequency transients in the mountain hemisphere.

The similarity between the EOF structures for the intermediate-frequency transients in the no-mountain simulation and those in the mountain simulations suggests that the generation mechanism of 10-day and wavenumber 5 eddies in the no-mountain hemisphere still operates in the hemisphere with orographic forcing. But the amplitude of these transients is modulated by the mountain and their propagation is affected. The reason that these transient eddies propagate equatorward in the upstream region of the mountain may be related to the refractive properties of the stationary waves. A zonal wavenumber 5 pattern with a timescale around 10 days has often been observed in the Southern Hemisphere (for example, Salby 1982). EOF analyses presented here suggest that those intermediate-scale waves are probably still generated in the Northern Hemisphere but are affected by the orographically forced stationary waves in such a way that they appear as equatorward propagating wave trains upstream of the mountain. This may account for the appearance of intermediate-frequency and equatorward-propagating wave trains observed in the Northern Hemisphere by Blackmon et al. (1983a,b). The appearance of the intermediate-scale waves at the downstream end of the track of high-frequency storms suggests that these lower-frequency, slightly larger scale disturbances may result from barotropic interactions during the later phases of the baroclinic wave lifecycle.

c. *Low-frequency transient eddies*

The leading EOF modes for the low-frequency transients are shown in Fig. 8. Unlike the higher-frequency modes, these EOFs do not show up in quadrature pairs. The leading EOF mode in the no-mountain simulation, as expected, exhibits a zonally symmetric and out of phase relation between low-frequency relative vorticity fluctuations in midlatitudes and those in lower and higher latitudes (Yu and Hartmann 1993). The correlation of the principal component of this mode with the principal component of the leading mode for the zonally averaged zonal wind is as high as 0.98. When a small mountain is introduced into the simulation, amplitude variations in the EOF mode are seen in the zonal direction. But the leading EOF modes in the mountain simulations retain a tendency for structural features to maintain a constant sign along latitude circles. An out of phase relation between middle latitudes and lower and higher latitudes, similar to the leading mode of the no-mountain simulation, remains in these mountain simulations. The amplitude is enhanced in the jet exit regions, and this enhancement is stronger in the higher mountain simulations. The smooth transition from the zonally symmetric structure to a more localized but zonally elongated structure in the 4-km mountain case suggests that the eddy–mean flow dynamics that were shown to cause the zonally symmetric pattern of variability may also have some relevance for the low-frequency variation downstream of jets.

To prove that the leading EOF mode shown in the 4-km mountain simulation is in part a similar zonal flow–eddy vacillation phenomenon as discussed in YH93, the composite and momentum budget analyses of YH93 are applied to this EOF mode. The composite zonal mean zonal wind and transient kinetic energy based on the highest and lowest 10% of the principal components of the leading EOF mode are shown in Fig. 9. In the low-index phase, the upper-level zonal mean wind is stronger and narrower and is located at 40°N. The high-index phase exhibits a weaker and broader composite wind in higher latitudes. Accompanying the variation in the jet, the storm track in the low-index phase is stronger and is located at a lower latitude. The storm track is weaker and shifts to higher latitudes in the high-index phase (Fig. 9b). Both the composite zonal flow and transient activity show typical relations seen in the zonal flow vacillation. Based on YH93, the zonal flow anomalies of two extreme phases of the leading low-frequency mode should be supported by the eddy momentum flux convergence from the synoptic timescale eddies. Hoskins et al. (1983) have shown that the acceleration of the mean flow induced by the transients through the momentum fluxes can be approximated by the divergence of the E vectors. The slightly different form of E vector (Hendon and Hartmann 1985), $E = [(v'^2 - u'^2)/2, -u'v']$, is used here. The primes indicate the transient components. With this form, the E vector is parallel to the intrinsic group velocity of barotropic Rossby waves on a zonal mean basic state. In Fig. 10, the difference of the horizontal divergence of the E vectors for high-frequency transients and the difference of zonal winds between the high and low index phases of the leading low-frequency mode are shown. Consistent with the momentum budget analyses in YH93, momentum flux forcing from high-frequency transients is in phase with the zonal flow anomalies. Figures 9 and 10 suggest that zonal flow vacillation resulting from wave–zonal flow interaction is still a dominant low-frequency phenomenon in the mountain hemisphere, but the phenomenon is localized in the jet exit region. The importance of high-frequency transient forcing to the zonal flow vacillation phenomenon is also consistent with the fact that the maximum low-frequency variability is coincident with the maximum high-frequency variability.

The dominance of the localized "zonal flow vacillation" in the mountain hemisphere was also found in other GCMs. Branstator (1990) showed that the second EOF mode for the monthly mean streamfunction at 300 mb in a perpetual January simulation of the CCM exhibits a zonally symmetric structure similar to the leading low-frequency mode in our 4-km mountain simulation. Branstator pointed out that this zonally symmetric mode of the CCM was not reproduced in his

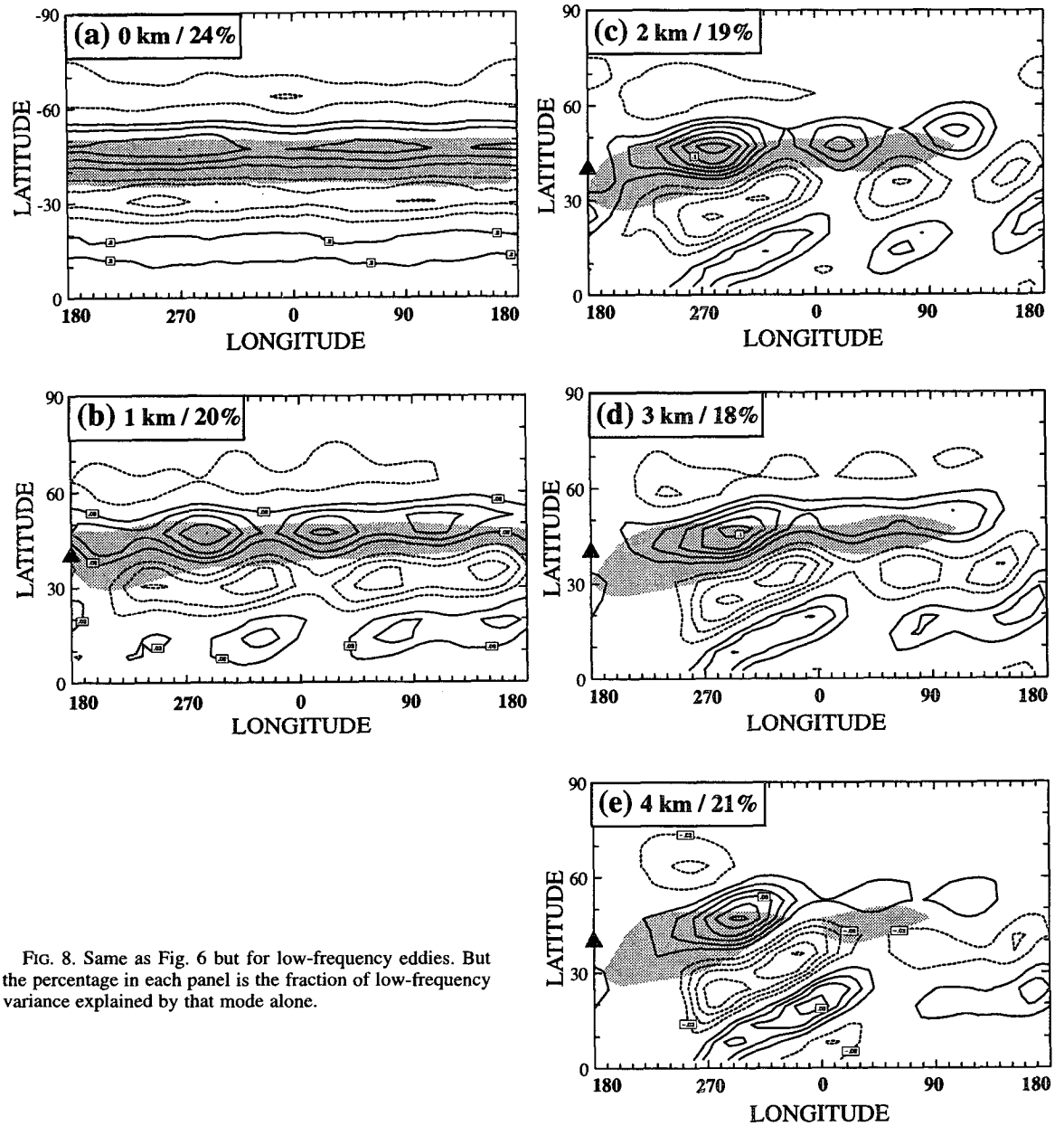

FIG. 8. Same as Fig. 6 but for low-frequency eddies. But the percentage in each panel is the fraction of low-frequency variance explained by that mode alone.

linear model. His later study (Branstator 1992) indicated that high-frequency transients play an important role in the maintenance of this mode. His results are consistent with the conclusions of YH93 and with our interpretation of the leading low-frequency mode in our mountain simulations.

5. Total amount of low-frequency variability and orographic forcing

Figure 4 indicates that the total amount of atmospheric variability seems to vary between the different mountain simulations. It has been suggested that the presence of large-scale mountains may affect the generation of low-frequency variability through internal dynamical processes, as well as provide new external generation mechanisms. In this section we examine the overall level of atmospheric variability in simulations with different mountain heights. The overall levels of variability are represented by the mass-weighted and meridionally and zonally averaged transient kinetic energy. The mass-weighted average is between 1000 and 200 mb, and the meridional average is from 0° to 90° in the mountain hemisphere. The averaged kinetic en-

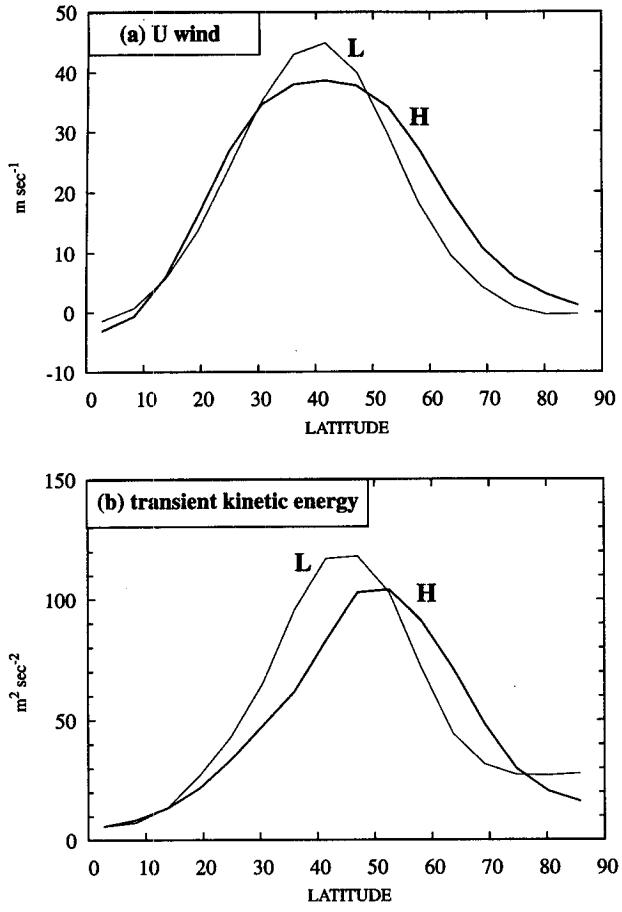

FIG. 9. Composite zonal mean zonal wind (a) and transient kinetic energy (b) for the leading EOF mode of the low-frequency transients in the 4-km mountain simulation. Zonal winds are calculated at 200 mb, and transient energies are calculated at 300 mb. The composites are calculated based on the days with the highest and the lowest 10% of the principal components of the leading EOF mode.

ergy for high-, intermediate-, and low-frequency eddies and stationary eddies from the no-mountain simulation and from the mountain simulations are listed in Table 1. It shows that the overall level of transient kinetic energy in the hemisphere decreases with increasing height of the mountain. At the same time, the energy of stationary eddies increases as the mountain is raised. The total amount of eddy energy, which is the sum of the transient and stationary eddy energy, is very nearly constant.

The variation of eddy kinetic energy in Table 1 suggests that orographic forcing causes a transfer of eddy energy from the transient component to the stationary component. One possible explanation to this transfer is the heat balance requirement in the hemisphere. In the atmosphere, eddy heat transport is necessary to prevent the thermal gradient from being continuously increased by radiative heating. In the simulations with orographic forcing, heat can be transported poleward by both the stationary eddies and the transient eddies. Since all the simulations are subject to the same equator to pole temperature forcing, the level of transient eddy activity required to transport heat in the mountain simulations is smaller than in the no-mountain simulation. To examine this argument, the overall levels of the eddy heat fluxes by transient and stationary eddies from all simulations are shown in Fig. 11. With a higher mountain in the simulation, the contribution from stationary eddies to heat transport is increased, and the heat transport by transient eddies is reduced by a similar amount. The total eddy heat flux by both the transient and stationary eddies appears to be almost the same for any mountain height.

The kinetic energies of the high-frequency and the intermediate-frequency transients both decrease as the height of the mountain is increased. For low-frequency transients, however, the kinetic energy is increased when the mountain is raised. Since the high and intermediate frequency transients contain the largest part of the transient eddy energy and their horizontal structures are meridionally elongated so that they produce efficient heat transport, the reduction of their kinetic energies in the simulations with higher mountains is consistent with the heat transport argument. The fractional changes of transient eddy kinetic energy with increasing mountain height are shown in Fig. 12. They are calculated as the ratios of transient eddy kinetic energy in the mountain simulations to that in the no-mountain simulation. The fractional decline of kinetic energy with increasing mountain height is faster for the high frequencies than for the total transient energy. Thus the heat transport argument cannot be a full explanation for the redistribution of transient variability seen in the mountain simulations. It appears that the efficiency with which the high-frequency transient energy is converted to lower frequencies is enhanced by the presence of strong zonal asymmetry or that the amount of low-frequency variability is controlled by something other than the rate at which eddy energy is produced at synoptic scales.

We have shown that zonal flow vacillation generated through interaction between zonal flows and high-frequency transients is an important low-frequency phenomenon in the mountain simulations. Since the amount of high-frequency transient energy decreases in the mountain simulations, low-frequency variability generated through the zonal flow–wave interaction might be expected to be less in the simulations with higher mountains, although a simple monotonic relationship between eddy energy intensity and the intensity of the zonal flow vacillation has not been demonstrated as yet. If so, the increase of low-frequency variability seen in Fig. 12 must be generated by other mechanisms. Barotropic instability associated with the orographically forced stationary waves and the direct interaction between the mountain and the zonal flow vacillation phenomenon are two such possible mecha-

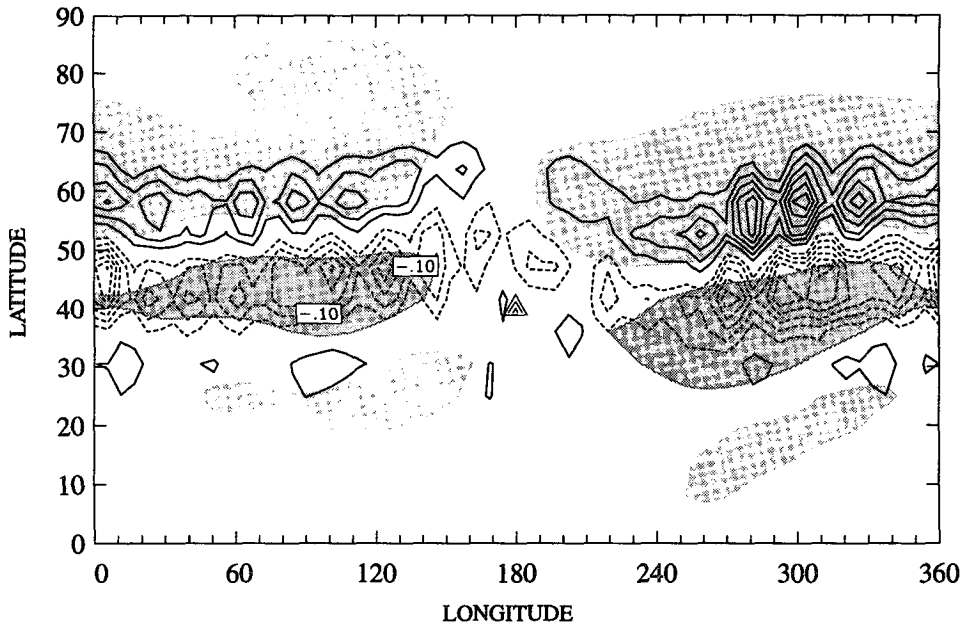

FIG. 10. Divergence difference of E-vector for high-frequency transients between the high- and the low-index phases of the leading low-frequency mode for the 4-km mountain simulation. The difference of composite zonal winds between two extreme phases of the EOF mode is shown by the shading. Light shading indicates large positive wind anomalies, while the dark shading indicates large negative anomalies. The contour interval is 5×10^{-6} m s^{-2}.

nisms. In this regard it is interesting to note that the low-frequency variability is the same in the 1-km mountain as the no-mountain simulation experiment, but then it increases significantly for the 2-km mountain case (Fig. 12). The low-frequency variability increases very slowly as the mountain height is increased beyond 2 km. This step increase suggests that the low-frequency variability increases dramatically as the stationary wave amplitude crosses a threshold and then becomes relatively insensitive to further increases in mountain height. The stationary kinetic energy increases linearly with mountain height from 0 to 2 km and then increases more slowly as the mountain height is increased further (Fig. 11). A similar saturation of the response of stationary waves to orographic forcing has been diagnosed by Cook and Held (1992).

6. Topography waveguides

In the previous sections, orographic influences on the geographical distribution of transient activity were discussed. The major influences of the large-scale mountain on the transient activity are primarily through the orographically forced stationary waves. The presence of stationary waves affects the propagation or the generation of transient eddies in various locations. It remains to be pointed out that there is a direct influence of a large-scale mountain on transient eddies. This direct influence occurs near the mountain areas and has little to do with the orographically forced stationary waves, but rather it depends on the presence of a sloping lower boundary. Figure 13 shows the horizontal distribution of kinetic energy for high-frequency tran-

TABLE 1. Eddy kinetic energy, mass-weighted from 1000 to 200 mb over the mountain hemisphere, from the no-mountain and the 1-km, 2-km, 3-km, and 4-km mountain simulations. The unit is m^2 s^{-2}.

Averaged eddy kinetic energy (m^2 s^{-2})	No mountain	1-km mountain	2-km mountain	3-km mountain	4-km mountain
Transient eddy	37.0	34.3	34.1	33.4	32.8
Stationary eddy	0.0	2.0	5.4	7.2	8.1
Total	37.0	36.3	39.5	40.6	40.9
High-frequency transient	16.2	13.8	12.8	11.9	11.5
Intermediate-frequency transient	11.4	10.9	10.7	10.6	10.2
Low-frequency transient	5.7	5.7	6.5	6.5	6.7

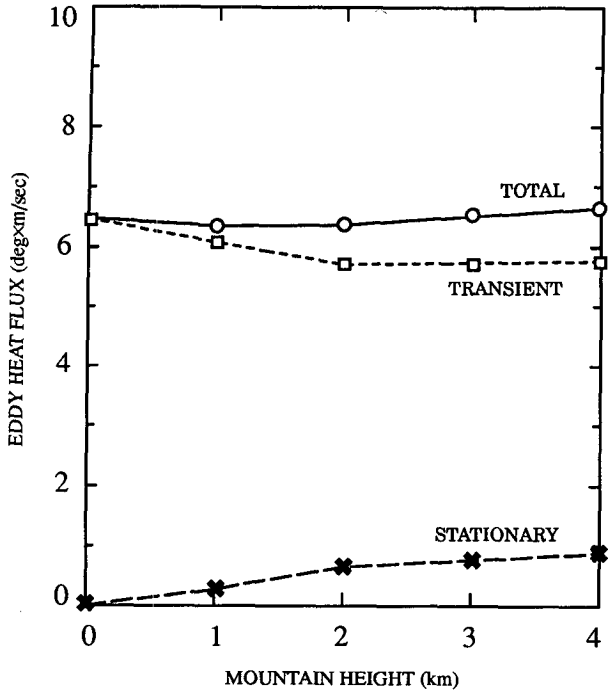

FIG. 11. Overall levels of eddy heat fluxes by transient and stationary eddies in the no-mountain simulation and in the mountain simulations. The overall levels of eddy heat flux are mass-weighted averages over the mountain hemisphere.

sients in the lower troposphere of the 4-km mountain hemisphere. Increased variability is seen in the region immediately downstream from the center of the mountain. This local variability maximum is confined to a narrow strip of longitude. The maximum extends into latitudes lower than the locations of other variance maxima. Examination of the vertical structure of this local maximum (not shown) indicates that it is confined in the low troposphere.

The propagation characteristics of high-frequency transient eddies in the near-mountain area are displayed with E vectors in Fig. 14. Strong equatorward propagation of high-frequency transients is clearly seen immediately downstream from the center of the mountain, where the high-frequency eddies can reach as far south as 20°N. There is also a tendency for the eddies to propagate along contours of constant surface elevation. This along-mountain propagation suggests that the mountain slope serves as a waveguide for the propagation of high-frequency transients in that region. A similar increase in high-frequency variability is seen in the 3- and 2-km mountain simulations, but not in the 1-km mountain simulation. Both the location and the shallowness of the topographic waveguide found in this GCM are similar to those observed in the real atmosphere (Hsu 1987). The increased equatorward transient activity near large mountain ranges has potential relevance for extratropical–tropical interaction. As shown in Fig. 14, these transients can propagate deep into the Tropics. Considering the large amount of moisture available in the lower troposphere of the Tropics, these equatorward-propagating extratropical disturbances might be capable of exciting deep convection in the Tropics. Atmospheric variability in the Tropics may be generated through this extratropical forcing. Therefore, large-scale mountains may also play an important direct role in extratropical–tropical interaction.

7. Summary and conclusions

This study employed GCM simulations to investigate orographic influences on atmospheric variability. The results suggested that not only the distribution but also the amount of atmospheric variability are affected by the presence of large-scale mountains. As the height of the mountain in the simulation is increased, three different timescales of variability become separated and are localized into different geographical locations. This scale separation phenomenon suggests that these three timescales may have different generation mechanisms or propagation characteristics. Orographic forcing and the stationary waves it generates thus have different effects on different timescales.

The maximum variability of high-frequency eddies appears in the region poleward of the jet stream and

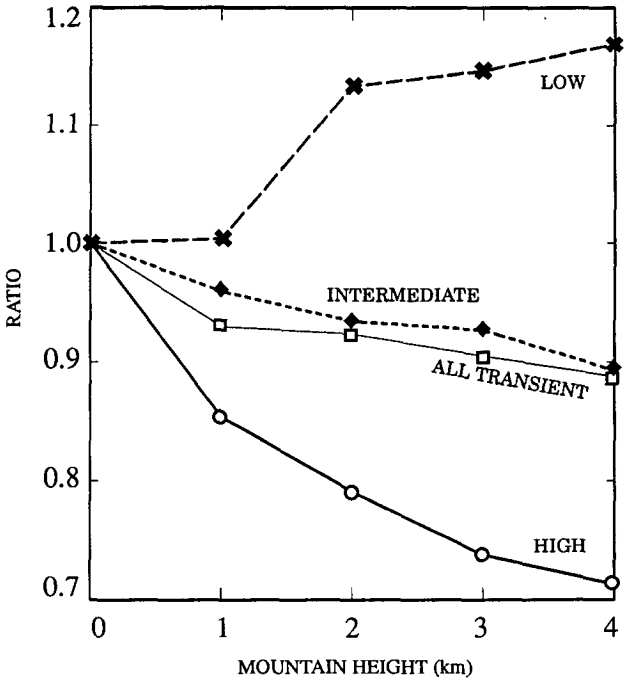

FIG. 12. Orographic dependence of overall levels of eddy kinetic energy for various frequency bands of transient eddies. The values plotted on the coordinate are the kinetic energy for transients in each simulations divided by the kinetic energy in the no-mountain simulation.

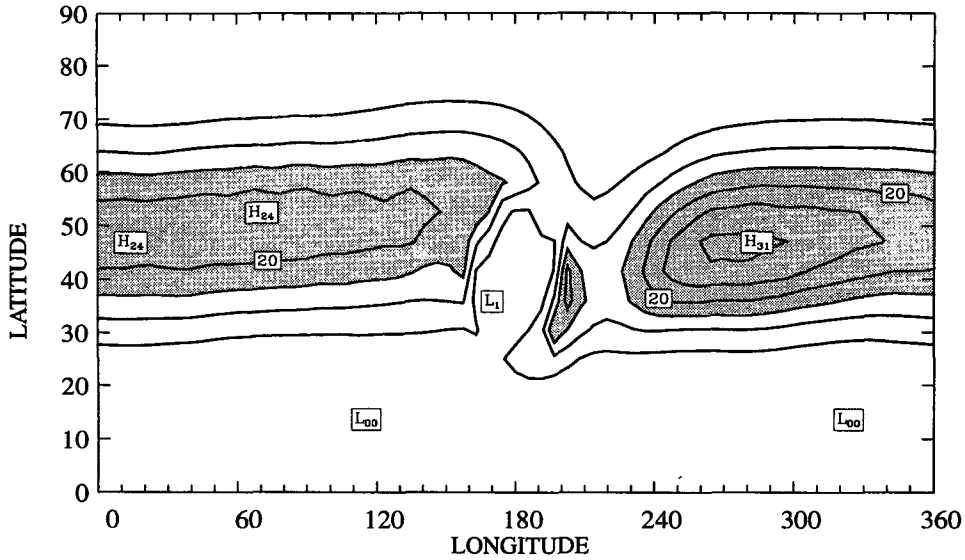

FIG. 13. Kinetic energy for high-frequency transients at 850 mb from the 4-km mountain simulation. Contour interval is 5 $m^2 s^{-2}$. Values greater than 15 $m^2 s^{-2}$ are shaded.

between the jet core and the jet exit. The dominant spatial pattern of the same timescales in the no-mountain hemisphere exhibits a global pattern of zonal wavenumber 6, but with increased orographic forcing this gradually changes to become a local wave packet structure in the 4-km mountain simulation. Comparisons among spatial structures in the no-mountain simulation and in the mountain simulations suggest that the amplitude of the global pattern of high-frequency transients in the no-mountain hemisphere is modulated by orographically forced stationary waves and appears as a local wave packet pattern in the mountain hemisphere. The amplitude modulation may be a result of the lifecycle development of baroclinic waves in the localized jets, followed by amplitude suppression of baroclinic eddies though deformation by the wind field variations associated with the stationary waves.

In contrast to the high-frequency eddies, intermediate-frequency eddies have their maximum amplitude upstream of the mountain, where they also exhibit en-

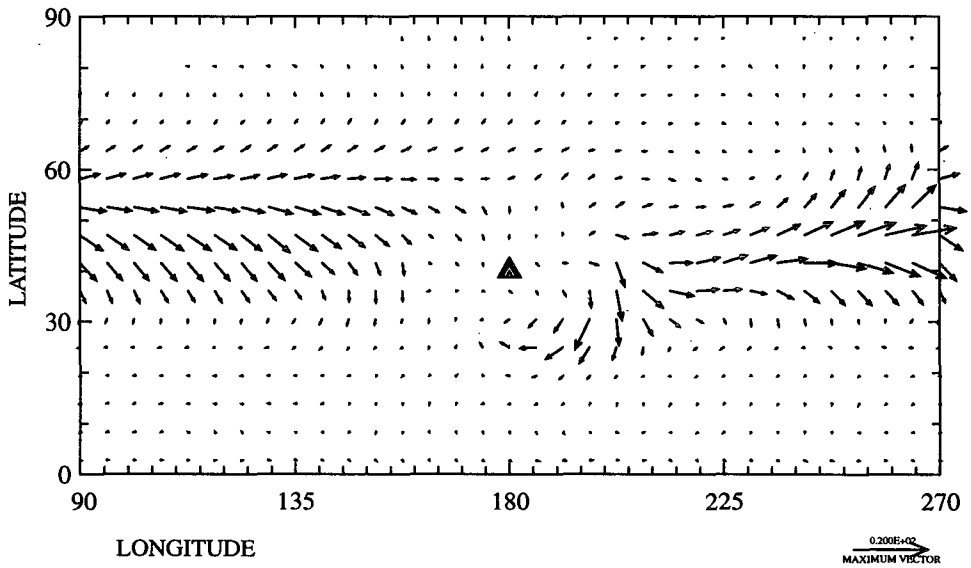

FIG. 14. E-vector of 7-day high-passed transient eddies on 850 mb from the 4-km mountain simulation. The triangular symbol indicates the center of the mountain.

hanced equatorward propagation. The dominant spatial structure for this timescale in the no-mountain hemisphere is a global wavenumber 5 pattern with a period near 10 days. With the presence of a large-scale mountain, a localized wave train structure with strong equatorward propagation near the upstream edge of the mountain appears as the dominant structure. This local wavetrain structure has a zonal scale of wavenumber 5 and a period near 12 days. It is suspected that the refractive properties of orographically forced stationary waves make the upstream edge of a mountain a preferred region for the collection and equatorward propagation of intermediate-frequency transients. It may be that these intermediate-scale transients result from the later stages of the baroclinic wave lifecycle when the structure evolves to be more barotropic and of larger scale. The position of the intermediate waves downstream of the high-frequency storm track is certainly consistent with this view. The analyses of the intermediate-frequency eddies in the zonally symmetric and very asymmetric simulations suggest that the intermediate timescale wave trains observed in the Northern Hemisphere may result from the same cause as the 10-day and wavenumber 5 eddies of the Southern Hemisphere (Salby 1982) but are more localized because of the jet structure and are forced equatorward in the jet entrance region.

In the case of the no-mountain simulation, the low-frequency structure is the same zonal flow vacillation pattern discussed in YH93. This pattern represents variations in the strength and the meridional location of the jet. With the presence of orographic forcing, the dominant low-frequency phenomenon in the mountain simulations is still the "zonally elongated" pattern but with a maximum amplitude in the storm track region. The localization of the zonal pattern in the region of maximum high-frequency variability is consistent with the conclusion that zonal flow vacillation is assisted by the interaction between the zonal flow and high-frequency eddies. Orographic forcing affects this part of low-frequency variability indirectly by the formation of storm tracks. The presence of zonal flow vacillation in the mountain simulations and the coherence of transient eddy forcing with this vacillation suggest that the wave–zonal flow interactions that dominate in zonally symmetric simulations may still be important in the Northern Hemisphere. A question that immediately follows this suggestion is whether the barotropic processes associated with the form drag instability (Charney and Devore 1979) or the interaction between baroclinic waves and zonal flow is more relevant to the variation of zonal index flow in the Northern Hemisphere's circulation.

This study also examined the influences of orographic forcing on the total amount of atmospheric variability. The results indicate that orographic forcing transfers eddy energy from the transient component to the stationary component, but the overall level of eddy kinetic energy is almost the same in all simulations. It is argued that atmospheres forced by the same equator to pole temperature forcing require similar eddy activity to provide the heat transport. Since the contribution from stationary eddies increases due to the presence of orographic forcing, the level of transient eddy activity required in the atmosphere is thus decreased. In contrast to the decreases in the amounts of high and intermediate frequency variability, the low-frequency variability increased with stronger orographic forcing. The simulations suggest a step function jump in low-frequency variability when the mountain is increased from 1 to 2 km in altitude, followed by much weaker increases as the mountain height is increased to 3 and 4 km. A rapid increase of low-frequency variability as the zonal asymmetry passes a critical threshold suggests the presence of a mechanism for generating low-frequency variability that is critically dependent on the degree of zonal asymmetry. Barotropic instability associated with east–west variations of flow is one possible mechanism (Simmons et al. 1983), but other mechanisms for generating low-frequency variability may also become more efficient when the flow is asymmetric and a large mountain is present. For example, the interaction of high-frequency transients with the time-mean flow is locally more intense in the region of a localized jet and may then be more efficient in generating quasi-stationary Rossby wave variability of low frequency.

A local influence of a large-scale mountain on the high-frequency atmospheric variability is seen in the lower troposphere on the downstream edge of the mountain. High-frequency variability is locally enhanced on the lee side of the mountain, and the high-frequency transient eddies propagate equatorward along the mountain slope. The large-scale mountain slope results in a mountain waveguide such that shallow extratropical disturbances can propagate into the Tropics. This equatorward propagation phenomenon is observed near the Himalayas and the Rockies in the real atmosphere and is believed to relate to cold surges.

Acknowledgments. The authors are grateful to two anonymous reviewers for comments on an earlier version of the manuscript. This research was supported by the Climate Dynamics Program, Atmospheric Sciences Division of the National Science Foundation under Grant ATM-93-13383. Computational support was supplied by the San Diego Supercomputer Center.

REFERENCES

Blackmon, M. L., Y. H. Lee, and J. M. Wallace, 1983a: Horizontal structure of 500-mb height fluctuations with long, intermediate, and short timescales. *J. Atmos. Sci.*, **41**, 961–979.

——, ——, ——, and H. H. Hsu, 1983b: Time variation of 500-mb height fluctuations with long, intermediate, and short timescales as deduced from lag-correlation statistics. *J. Atmos. Sci.*, **41**, 981–991.

Branstator, G., 1983: Horizontal energy dispersion in a barotropic atmosphere with meridional and zonal structures. *J. Atmos. Sci.*, **40,** 1689–1708.

——, 1990: Low-frequency patterns induced by stationary waves. *J. Atmos. Sci.*, **47,** 629–648.

——, 1992: The maintenance of low-frequency atmospheric anomalies. *J. Atmos. Sci.*, **49,** 1924–1945.

Charney, J. G., and J. G. DeVore, 1979: Multiple flow equilibria in the atmosphere and blocking. *J. Atmos. Sci.*, **36,** 1205–1216.

Cook, K. H., and I. M. Held, 1992: The stationary response to large-scale orography in a general circulation model and a linear model. *J. Atmos. Sci.*, **49,** 525–539.

Frederiksen, J. S., 1983: Disturbances and eddy fluxes in Northern Hemisphere flows: Instability of three-dimensional January and July flows. *J. Atmos. Sci.*, **40,** 836–855.

Hendon, H. H., 1986: Time-mean flow and variability in a nonlinear model of the atmosphere with orographic forcing. *J. Atmos. Sci.*, **43,** 432–448.

——, and D. L. Hartmann, 1985: Variability in a nonlinear model of the atmosphere with zonally symmetric forcing. *J. Atmos. Sci.*, **42,** 2783–2797.

Hoskins, B. J., and T. Ambrizzi, 1993: Rossby wave propagation on a realistic longitudinally varying flow. *J. Atmos. Sci.*, **50,** 1661–1671.

——, I. N. James, and G. H. White, 1983: The shape, propagation, and mean-flow interaction of large-scale weather systems. *J. Atmos. Sci.*, **40,** 1595–1612.

Hsu, H.-H., 1987: Propagation of low-level circulation features in the vicinity of mountain ranges. *Mon. Wea. Rev.*, **115,** 1864–1892.

——, and J. M. Wallace, 1985: Vertical structure of wintertime teleconnection patterns. *J. Atmos. Sci.*, **42,** 1693–1710.

Lee, S., and I. M. Held, 1993: Baroclinic wave packets in models and observations. *J. Atmos. Sci.*, **50,** 1413–1428.

Pierrehumbert, R. T., 1984: Local and global baroclinic instability of a zonally varying flow. *J. Atmos. Sci.*, **41,** 2141–2162.

Robert, A. J., J. Henderson, and C. Turnbull, 1972: An implicit time integration scheme for baroclinic models of the atmosphere. *Mon. Wea. Rev.*, **100,** 329–335.

Salby, M. L., 1982: A ubiquitous wavenumber-5 anomaly in the Southern Hemisphere during FGGE. *Mon. Wea. Rev.*, **110,** 1712–1720.

Simmons, A. J., J. M. Wallace, and G. W. Branstator, 1983: Barotropic wave propagation and instability and atmospheric teleconnection patterns. *J. Atmos. Sci.*, **40,** 1363–1392.

Wallace, J. M., 1983: The climatological mean stationary waves: Observational evidence. *Large-scale Dynamical Processes in the Atmosphere,* B. Hoskins and R. Pearce, Eds., Academic Press, 397 pp.

Yu, J.-Y., 1993: The roles of wave-zonal flow interaction and orographic forcing on the generation of low-frequency variability in a newly developed GCM. Ph.D. Dissertation, University of Washington, Seattle, 236 pp.

——, and D. L. Hartmann, 1993: Zonal flow vacillation and eddy forcing in a simple GCM of the atmosphere. *J. Atmos. Sci.*, **50,** 3244–3259.